IEEE Access
Multidisciplinary | Rapid Review | Open Access Journal

Received August 28, 2019, accepted September 3, 2019, date of publication September 6, 2019, date of current version September 20, 2019.

Digital Object Identifier 10.1109/ACCESS.2019.2939759

Research on Deadbeat Current Prediction Vector Control System of Axial Flux Permanent Magnet Synchronous Motor for Electric Bus Based on Efficiency Optimal Torque Distribution Method

JIANFEI ZHAO, LIXIAO ZHENG, SHUANG WANG, AND MINQI HUA
School of Mechatronic Engineering and Automation, Shanghai University, Shanghai 200444, China

Corresponding author: Jianfei Zhao (jfzhao@shu.edu.cn)

This work was supported by the Shanghai Natural Science Foundation under Grant 19ZR1418600.

ABSTRACT In order to improve the cruising range of electric bus, this paper studies the deadbeat current prediction vector control system of axial flux permanent magnet synchronous motor (AFPMSM) for electric bus based on the optimal torque distribution method. Firstly, the mathematical model of the three stators-double rotors AFPMSM is established. Secondly, in order to improve the high efficiency range, the efficiency optimal torque distribution method is proposed based on the average torque distribution method and the back propagation (BP) neural network is used to find the optimal torque distribution method. Then a current control strategy based on deadbeat current prediction control is proposed to improve the torque tracking characteristics. Finally, a drive control system is developed for the proposed control strategy, and experimental research and vehicle testing are carried out. The experimental results show that the BP neural network-based torque distribution method designed in this paper increases the high efficiency range of the drive system and improves the cruising range of the electric bus. The drive system using a current controller based on deadbeat current prediction control exhibits good dynamic and steady state performance.

INDEX TERMS Electric bus, AFPMSM, BP neural network, efficiency optimal torque distribution, deadbeat current prediction control.

I. INTRODUCTION

New energy vehicles can be used in the public transportation sector to achieve energy conservation and emission reduction and to develop local new energy vehicle industry [1], [2], in which electric buses have been initially applied. The drive motor is an important part of the electric bus. The application of the drive motors have two main trends in the world, the alternating current asynchronous motor and the permanent magnet synchronous motor (PMSM). Among them, the PMSMs have a wide coverage of power level, which can fully meet the power demand of the electric bus. The current research on PMSMs have been deepened. The authors of [3] conducted model prediction torque control for PMSMs for electric vehicles. The authors of [4] performed torque analysis on the PMSM for electric vehicles and improved the dynamic performance. Torsional vibration analysis and modeling of hybrid electric vehicles are carried out in [5], [6]. In PMSMs, axial flux permanent magnet synchronous motors (AFPMSMs) have been widely used due to their high power factor, high efficiency, high power density and compact structure [7], [8]. The literature [9]–[14] applied AFPMSMs to large-scale wind power, electric vehicles, electric bicycle, electric motorcycle, robot and left ventricular assist device, respectively. In summary, AFPMSM is suitable for using as an high power drive motor on an electric bus. A three-stator-double-rotor AFPMSM is used in this paper, which has three independent stator windings, which can be equivalent to three identical motors by decoupling. The axial connection is coaxial with a plurality of ordinary motors, and has the advantages

The associate editor coordinating the review of this manuscript and approving it for publication was Xiaosong Hu.

of low cost, simple structure, small occupied space and the like.

The difference between electric buses and traditional buses is the energy system and the transmission system. For the energy system, many researchers have conducted in-depth research on vehicle scheduling and energy management strategies for electric buses. Since the bus departure time is based on the timetable, the authors of [15]–[17] conducted a detailed study on the electric bus vehicle scheduling. Secondly, since the driving route of the bus is fixed, the energy management strategy can be used to ensure the efficiency of the electric bus. The authors of [18]–[20] used different methods to manage energy in electric buses.

Another research focus of electric buses is the transmission system. The research on the transmission system is also divided into cruising range research, torque distribution research, drive control method research and so on. Literature [21], [22] used different methods to improve the cruising range of electric vehicles. Gan C, Jin N, Sun Q, *et al.* proposed a multiport bidirectional switched reluctance motor drive for solar-assisted hybrid electric bus powertrain, which not only improves the motoring performance, but also achieves flexible charging functions [21]. Li J, Zhang M, Yang Q, *et al.* proposed a superconductor magnetics energy storage/battery hybrid energy storage system used in electrical buses with the benefit of extending battery lifetime [22]. In [23]–[26], the drive system of electric vehicles was studied. Zhang D, Zhang S, Fan T, et al. studied the interference coupling mechanism between the electric vehicle and low voltage circuit in an electric vehicle motor drive system [23]. Li C, Huang W, Cao R, et al. modelled an integrated topology of the charger and drive for medium/high power electric buses [24]. Zhao J, Hua M, Liu T proposed a sliding mode vector control system based on collaborative optimization of an AFPMSM for an electric vehicle [25]. The grey wolf optimization algorithm is used to control the permanent magnet synchronous hub motor in [26]. In addition, the authors of [27], [28] conducted a detailed study of the torque distribution of electric vehicles.

For electric buses, in addition to energy management, the most important thing is the cruising range. Therefore, it is very necessary to use better control methods to improve the cruising range of electric buses. In addition, electric buses are an important part of public transportation, so their drive systems must have good control accuracy and stability so that they can drive safely on the road. In summary, this paper has conducted in-depth research on improving the cruising range of electric buses and the performance of the drive control system. Firstly, based on the torque average distribution strategy, the optimal torque distribution strategy is proposed. The BP neural network is used to find the torque distribution method that makes the three-stator-double-rotor AFPMSM the optimal. In order to improve the accuracy and performance of the electric bus drive control system studied in this paper, a current control strategy based on deadbeat current prediction control is proposed to improve the torque tracking characteristics.

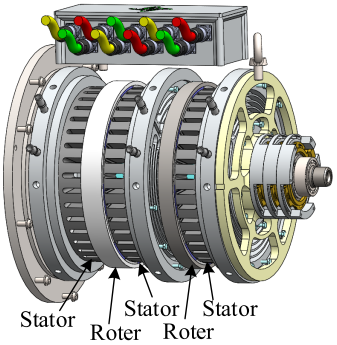

FIGURE 1. Three-disc AFPMSM three-dimensional structure diagram.

The main structure of this paper is as follows: In the first section, the mathematical model of the three-stator-double-rotor AFPMSM is deduced. In the second section, the optimal torque distribution method based on BP neural network algorithm is proposed and studied. In the third section, a current control strategy based on deadbeat current prediction control is proposed, and the drive control system for electric buses is studied. In the fourth section, experimental research and vehicle testing are conducted. In the fifth section, this article is summarized.

II. MATHEMATICAL MODEL OF A THREE-DISC AFPMSM

The three-stator-double rotor AFPMSM, which is also called three-disc AFPMSM, three-dimensional structure is shown in Figure 1. Since the main magnetic flux equivalent magnetic circuits of adjacent stators and rotors are independent of each other, the interaction between the three sets of stator windings and between the two rotor disks are ignored. At this time, the three-disc AFPMSM can be equivalent to the case where three PMSMs are coaxially connected, and each set of stator windings can be independently controlled. A set of stator windings is selected to establish a mathematical model. Referring to the derivation process of the mathematical model of the ordinary PMSM, the mathematical model of the three-disc AFPMSM in the three-phase stationary coordinate system is as follows [29]:

Voltage equation:

$$\begin{bmatrix} u_A \\ u_B \\ u_C \end{bmatrix} = \begin{bmatrix} R_s & 0 & 0 \\ 0 & R_s & 0 \\ 0 & 0 & R_s \end{bmatrix} \begin{bmatrix} i_A \\ i_B \\ i_C \end{bmatrix} + p \begin{bmatrix} \psi_A \\ \psi_B \\ \psi_C \end{bmatrix} \quad (1)$$

where u_A, u_B, u_C are the stator voltage, i_A, i_B, i_C is the stator current in the A-B-C coordinate system, and ψ_A, ψ_B, ψ_C is the stator flux linkage in the A-B-C coordinate system. R_s is the stator winding resistance. p is the differential operator (d/dt).

Flux equation:

$$\begin{bmatrix} \psi_A \\ \psi_B \\ \psi_C \end{bmatrix} = \begin{bmatrix} L_{AA} & M_{AB} & M_{AC} \\ M_{BA} & L_{BB} & M_{BC} \\ M_{CA} & M_{CB} & L_{CC} \end{bmatrix} \begin{bmatrix} i_A \\ i_B \\ i_C \end{bmatrix} + \begin{bmatrix} \cos\theta \\ \cos(\theta - 120°) \\ \cos(\theta + 120°) \end{bmatrix} \psi_r \quad (2)$$

where L_{XX} is the self-inductance of the X-phase winding, M_{YY} is the mutual inductance between the stator windings X and Y, ψ_r is the rotor permanent magnet flux linkage, θ is the rotor position angle.

Torque equation:

$$T_e = N_p \psi_s \times i_s \tag{3}$$

where T_e is the electromagnetic torque, N_p is the pole pair number of the torque winding, ψ_s is the stator flux vector, i_s is the stator current vector.

Equation of motion:

$$Jp\left(\frac{\omega_r}{N_p}\right) + B\left(\frac{\omega_r}{N_p}\right) = T_e - T_L \tag{4}$$

where J is the motor moment of inertia, B is the viscosity coefficient, T_L is the load torque, and ω_r is the rotor angular velocity.

The above equation shows that the mathematical model of AFPMSM in the A-B-C coordinate system is a set of linear differential equations with variable coefficients. In order to facilitate the analysis, it is usually converted into a mathematical equation in the d-q axis coordinate system by coordinate transformation. The mathematical equations in the d-q axis coordinate system are as follows:

d-q axis voltage equation:

$$u_d = R_s i_d + p\psi_d - \omega_r \psi_q \tag{5}$$

$$u_q = R_s i_q + p\psi_q + \omega_r \psi_d \tag{6}$$

where u_d, i_d is the component of the stator voltage and current vector in the d-axis, u_q, i_q is the component of the stator voltage and current vector in the q-axis

d-q axis stator flux equation:

$$\psi_d = L_d i_d + \psi_f \tag{7}$$

$$\psi_q = L_q i_q \tag{8}$$

where ψ_f is the flux of the permanent magnet fundamental excitation field coupled to the stator winding, ψ_d, ψ_q is the air gap magnetic field in the d-axis and q-axis component, L_d, L_q is the self-inductance of the d-axis and q-axis coil.

Because the AFPMSM does not have a salient pole effect, and $L_d = L_q$, the torque equation is obtained:

$$T_e = \frac{3}{2} N_p \psi_f i_q \tag{9}$$

Since the three sets of stators jointly drive two rotor disks, the two rotor disks are coaxially connected, and the motor is structurally equivalent to three motor shafts. Therefore, the reference coordinate systems corresponding to the three stators are identical. At this point, the motors corresponding to the three stators can be analyzed by placing them in the same d-q reference coordinate system. Since the three stators are identical in structure and have symmetry, $R_s = R_{s1} = R_{s2} = R_{s3}$, and the motor air gap is uniform, that is, $L_q = L_{q1} = L_{q2} = L_{q3}$. At this point, the electromagnetic torque equation can be rewritten as:

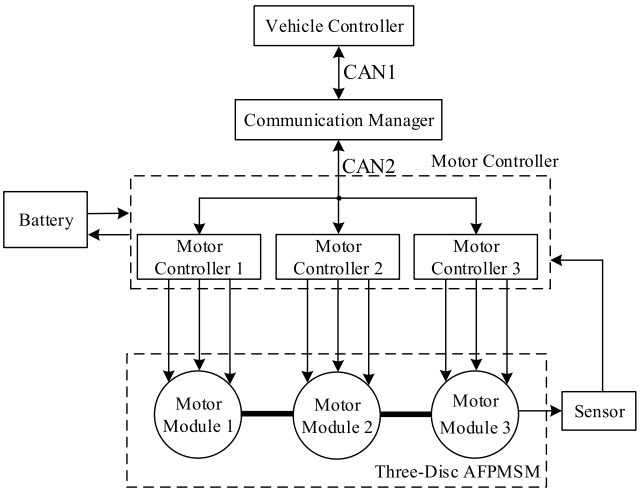

FIGURE 2. Three-disc AFPMSM drive system topology for electric buses.

$$T_e = T_{e1} + T_{e2} + T_{e3} = \frac{3}{2} N_p \psi_f \left(i_{q1} + i_{q2} + i_{q3}\right) \tag{10}$$

where T_e is the total electromagnetic torque of the motor, T_{e1}, T_{e2}, T_{e3} are the electromagnetic torques of the stator 1, 2 and 3 windings respectively, i_{q1}, i_{q2}, i_{q3} are the components of the stator 1, 2 and 3 winding current vectors in the q-axis.

III. EFFICIENCY OPTIMAL TORQUE DISTRIBUTION METHOD BASED ON BP NEURAL NETWORK

A. TOPOLOGY OF THREE-DISC AFPMSM DRIVE SYSTEM

The structure of the three-disc AFPMSM drive system used in this paper is different. The topology of the drive system is shown in Figure 2. Although an electric bus only needs a three-disc AFPMSM drive, since the motor has three sets of independent stator windings, the drive system requires three sets of motor controllers for control. In order to increase the general performance of the three-disc AFPMSM drive system, the conventional vehicle controller can also be applied in the three-disc AFPMSM drive system, usually using a communication manager. The command of the vehicle controller is first sent to the communication manager, and after the communication manager determines the working state and the torque magnitude of the plurality of motor modules according to the preset control strategy, the control signal and the torque data are distributed to the three motor modules. At the same time, the three motor modules first send the feedback motor state information to the communication manager, and the communication manager integrates the plurality of motor module state information into overall motor state information and sends it to the vehicle manager, so that in the case of a car manager, it is equivalent to controlling a conventional motor.

Electric buses generally operate in torque mode, and control the output of the motor torque according to the depth at which the driver steps on the throttle. The torque distributor

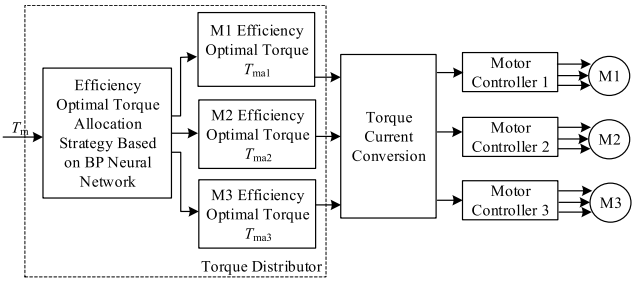

FIGURE 3. Torque distribution control block diagram.

included in the communication manager is first studied in this section. In general multi-motor systems, the torque average distribution is used to distribute the total torque T_m. In order to further improve the system efficiency, this section studies the efficiency optimal torque distribution method based on BP neural network. The most efficient torque distribution method is obtained by BP neural network optimization in this method. Firstly, the optimal torques T_{ma1}, T_{ma2} and T_{ma3} of motor 1, motor 2 and motor 3 are obtained by the optimal torque distribution method based on BP neural network, and then reach the motor controller through torque current conversion. The torque distributor structure diagram is shown in Figure 3.

B. EFFICIENCY OPTIMAL TORQUE DISTRIBUTION METHOD BASED ON BP NEURAL NETWORK

Because the driving conditions of electric buses are affected by many factors, the collected data is relatively large, so this paper uses intelligent algorithms to optimize. Assume that the output torque of the three-disc AFPMSM is T, which belongs to [0,990 Nm]; the output torques of the three sets of motor modules are T_1, T_2 and T_3, respectively, belonging to [0,330 Nm], and there are constraints:

$$T = T_1 + T_2 + T_3 \tag{11}$$

The mechanical angular velocity of the motor is ω, and then the mechanical power output of the three sets of motor modules is $T_1\omega$, $T_2\omega$, $T_3\omega$. When the speed is ω and the torque is T_1, T_2, T_3, the corresponding single-group motor module efficiency is η_1, η_2 and η_3, respectively, so that $T_1 = a_1T$, $T_2 = a_2T$, $T_3 = a_3T$, where a_1, a_2, a_3 belong to [0,1], and $a_1 + a_2 + a_3 = 1$, the corresponding input power of each group of motor modules are:

$$P_1 = \frac{T_1\omega}{\eta_1} = \frac{a_1}{\eta_1}T\omega \tag{12}$$

$$P_2 = \frac{T_2\omega}{\eta_2} = \frac{a_2}{\eta_2}T\omega \tag{13}$$

$$P_3 = \frac{T_3\omega}{\eta_3} = \frac{a_3}{\eta_3}T\omega \tag{14}$$

The total input power is:

$$P_i = P_1 + P_2 + P_3 = (\frac{a_1}{\eta_1} + \frac{a_2}{\eta_2} + \frac{a_3}{\eta_3})T\omega \tag{15}$$

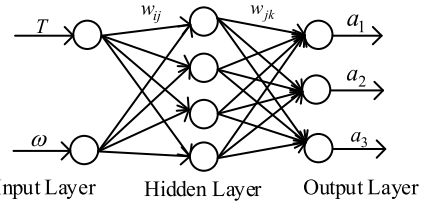

FIGURE 4. BP neural network topology for torque distribution.

The total output power is:

$$P_o = T\omega \tag{16}$$

System efficiency is:

$$\eta = \frac{P_o}{P_i} = \frac{T\omega}{(\frac{a_1}{\eta_1} + \frac{a_2}{\eta_2} + \frac{a_3}{\eta_3})T\omega} = \frac{1}{\frac{a_1}{\eta_1} + \frac{a_2}{\eta_2} + \frac{a_3}{\eta_3}} \tag{17}$$

Since the total torque T and the rotational speed ω are constant at a certain moment, the total output power is constant. To improve the system efficiency, only the total input power needs to be reduced, that is, the P_i is decreased. Let $A = a_1/\eta_1 + a_2/\eta_2 + a_3/\eta_3$. Finding the minimum value of P_i is converted to finding the values of a1, a2, and a3 such that A is the minimum value.

In this paper, a three-layer BP neural network is used, in which the input layer contains two neurons, the output layer contains three neurons, and the hidden layer contains four neurons. The structure is shown in Figure 4. The two input quantities of the input layer are the total torque T and the rotational speed ω, respectively, and the states of the three neurons of the output layer correspond to three parameters a_1, a_2, and a_3.

The calculation formula for the hidden layer is:

$$S_j = f(\sum_{i=1}^{n} X_i w_{ij} - \theta_j) \tag{18}$$

The output of the hidden layer neurons is excited by the S function:

$$f(x) = \frac{1}{1 + e^{-x}} \tag{19}$$

The calculation formula for the network output is:

$$Y_k = g(\sum_{i=1}^{n} S_j w_{jk} - r_k) \tag{20}$$

The output of the output layer neurons is also excited by the S function:

$$g(x) = \frac{1}{1 + e^{-x}} \tag{21}$$

The network output and ideal output error are:

$$e_k = Q_k - Y_k \tag{22}$$

The specified error performance indicator function is:

$$E_k = \frac{1}{2}e_k^2 \tag{23}$$

In the case of considering the shorter iteration time, the weighting coefficient of the network is modified according to the gradient descent method, that is, the weighting coefficient is searched and adjusted in the negative gradient direction according to the performance index function, and the connection weight learning algorithm of the output layer and the hidden layer is:

$$\Delta w_{jk} = -\eta \frac{\partial E_k}{\partial w_{jk}} = -\eta \cdot e_k \cdot \frac{\partial Y_k}{\partial w_{jk}} = -\eta \cdot e_k \cdot Y_k^{'} \quad (24)$$

The η in the above equation is called the learning rate, and is a preset constant for controlling the speed of the connection weight adjustment. It can be seen from the formula of the gradient descent algorithm that when the error tends to zero, $\partial E_{\mathrm{k}}/\partial w_{\mathrm{jk}}$ will tend to zero, which will cause the connection weight to be no longer updated, and the weight obtained at this time is the optimal information learned by the neural network.

The connection weight between the output layer and the hidden layer at time t+1 is:

$$w_{jk}(t+1) = w_{jk}(t) + \Delta w_{jk} \quad (25)$$

The hidden layer and input layer connection weight learning algorithm is:

$$\Delta w_{ij} = -\eta \frac{\partial E_k}{\partial w_{ij}} = -\eta \cdot e_k \cdot \frac{\partial Y_n}{\partial w_{ij}} \quad (26)$$

At t + 1, the hidden layer and input layer connection weights are:

$$w_{ij}(t+1) = w_{ij}(t) + \Delta w_{ij} \quad (27)$$

When using the gradient descent algorithm, sometimes the error will fluctuate back and forth within a certain range, because the η setting is too large. When η is set too small, the error will enter the local minimum point. After reaching the local minimum point, the gradient value Δw will tend to zero, which is generally called the gradient disappearing phenomenon, which will make the performance function unable to reach the global optimum. In order to prevent the error from going back and forth over a wide range of fluctuations and the phenomenon of gradient disappearance, a momentum factor $\alpha(0 < \alpha < 1)$, is added to the gradient descent method. Herein, α is taken as 0.05.The weight change amount becomes

$$\Delta w(t+1) = -\eta \frac{\partial E_k}{\partial w} + \alpha \Delta w(t) \quad (28)$$

As can be seen from the above equation, the change in the current weight is related to the change in the previous weight. If $\Delta w(t) > 0$, the current weight change is correct, and the change of the weight can be accelerated; if $\Delta w(t) < 0$, the current weight is suppressed from continuing to change in the wrong direction. This can effectively suppress the error fluctuation and enter the local minimum.

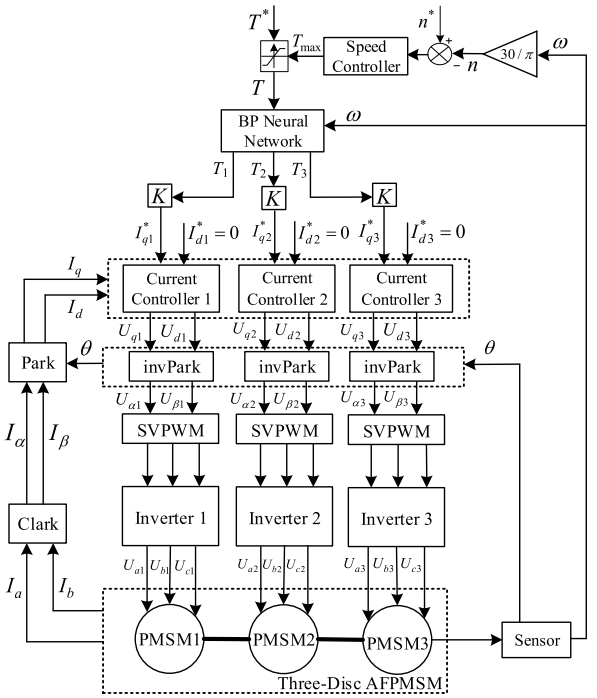

FIGURE 5. Electric bus vector control system block diagram.

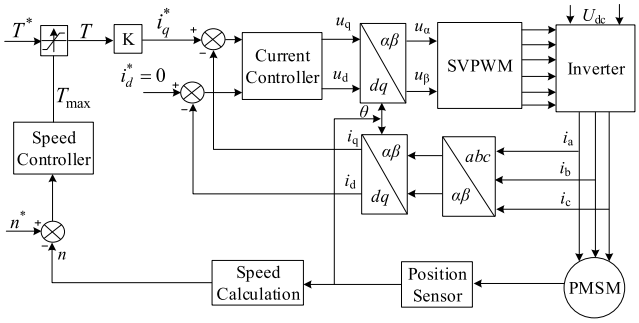

FIGURE 6. Control system block diagram.

IV. THREE-DISC AFPMSM DRIVE CONTROL STRATEGY BASED ON DEADBEAT CURRENT PREDICTION

Electric buses generally work in torque mode. The traditional double-closed vector control structure of speed and current is not suitable for use in electric bus motor drive control systems. According to the requirements of electric motor drive control system for motor output torque and speed limit, the structure diagram of the three-disc AFPMSM vector control system for electric bus designed in this paper is shown in Figure 5.

In order to facilitate the analysis, the single-disk control system in the three-disc AFPMSM is taken as the control object, and the vector control strategy is studied. The block diagram of the single-disk control system is shown in Figure 6. The single disc control system includes a speed loop and two current loops, where T^* is a given torque, T is a given torque after limiting, $T_{\max}$ is the output of the speed controller, and K is the conversion coefficient of torque and

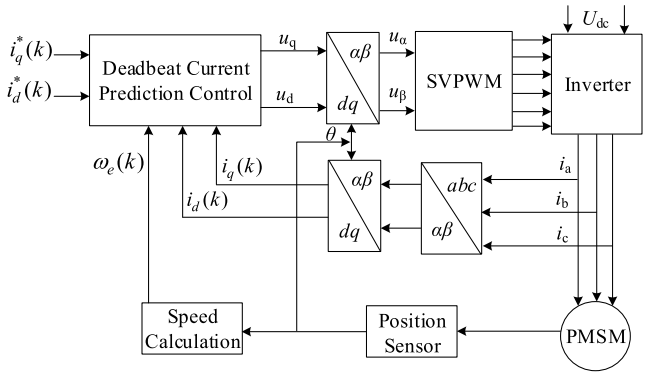

FIGURE 7. Schematic diagram of no beat current prediction control.

q-axis current, the value of which is related to the motor parameters. The control requirement for the current loop is to have the output torque follow a given torque. Different from the traditional speed controller, the speed loop of this paper is the speed limit loop. The control requirement of the speed loop is to make the motor speed not exceed the maximum speed, which is achieved by limiting the amplitude of the given torque T^*. When the motor speed is lower than the maximum speed, the speed loop does not work, the system works in the current single closed loop mode; when the throttle command is too large or the vehicle is over speed, the system works in the speed and current double closed loop mode, so that the motor does not exceed the maximum speed.

In order to improve the dynamic response and steady-state response of the motor current loop, a current controller based on deadbeat current prediction control is designed. The schematic diagram of the deadbeat current prediction control is shown in Figure 7. Because the algorithm combines spatial modulation technology, its voltage utilization is high, and the switching frequency is fixed and the current response speed is fast. The mathematical model is derived below.

According to the mathematical model of the three-disc permanent magnet synchronous motor, the voltage equation under the d and q axes is

$$\begin{bmatrix} u_d \\ u_q \end{bmatrix} = R_s \begin{bmatrix} i_d \\ i_q \end{bmatrix} + L \begin{bmatrix} \frac{i_d}{dt} \\ \frac{i_q}{dt} \end{bmatrix} + \begin{bmatrix} -\omega_e L i_q \\ \omega_e L i_d + \omega_e \psi_f \end{bmatrix} \tag{29}$$

where u_d, i_d is the component of the stator voltage and current vector on the d-axis, u_q, i_q is the component of the stator voltage and current vector in the q-axis, ψ_f is the flux linkage of the permanent magnet fundamental excitation field coupled to the stator winding, R_s is the stator winding resistance and L is the synchronous inductor, ω_e is the electrical angular velocity.

Using the current of the motor as a state variable, the equation of state for a three-disc AFPMSM can be obtained:

$$\begin{cases} \dfrac{di_d}{dt} = \dfrac{u_d}{L} - \dfrac{R}{L} i_d + i_q \omega_e \\ \dfrac{di_q}{dt} = \dfrac{u_q}{L} - \dfrac{R}{L} i_q - i_d \omega_e - \psi_f \omega_e \end{cases} \tag{30}$$

When the sampling period T is small enough, the first-order Taylor equation can be used to discretize the current state equation. Herein, T = 1μs.The following formula can be approximated:

$$\begin{cases} \dfrac{di_d}{dt} = \dfrac{i_d(k+1) - i_d(k)}{T} \\ \dfrac{di_q}{dt} = \dfrac{i_q(k+1) - i_q(k)}{T} \end{cases} \tag{31}$$

Bring (30) into (31), the discretized current prediction model can be got:

$$\begin{cases} i_d(k+1) = T_s \dfrac{1}{L}[u_d(k) - R i_d(k) + L\omega_e(k) i_q(k)] + i_d(k) \\ i_q(k+1) = T_s \dfrac{1}{L}[u_q(k) - R i_q(k) - L\omega_e(k) i_d(k) \\ \qquad\qquad - L\psi_f \omega_e(k)] + i_q(k) \end{cases} \tag{32}$$

The given signal current quantities $i_\mathrm{d}*$ and $i_\mathrm{q}*$ are used as input quantities $i_\mathrm{d}(k+1)$ and $i_\mathrm{q}(k+1)$ at the next time $T(k+1)$. The three-phase stator currents obtained by the acquisition are transformed by the mathematical coordinate system to obtain the current quantities i_d and i_q at the time $T(k)$, and the optimal voltage vectors u_d and u_q of the equation (33) can be obtained by combining the equations (30). Then, through the SVPWM modulation technology, a switching pulse for controlling the inverter is generated, thereby realizing the fast response control of the current loop, so that the actual current follows the given current after one sampling period. When the sampling period is small enough, it can be considered that there is no beat following the given signal.

$$\begin{cases} u_d(k) = L\left(\dfrac{i_d^*(k) - i_d(k)}{T_s}\right) + R i_d(k) - L\omega_e(k) i_q(k) \\ u_q(k) = L\left(\dfrac{i_q^*(k) - i_q(k)}{T_s}\right) + R i_q(k) + L\omega_e(k) i_q(k) + \psi_f \omega_e(k) \end{cases} \tag{33}$$

V. SIMULATION AND EXPERIMENTAL RESEARCH ON ELECTRIC BUS DRIVE SYSTEM

A. SIMULATION RESEARCH ON ELECTRIC BUS DRIVE SYSTEM

Using the BP neural network-based torque distribution method and the deadbeat current prediction controller designed in this paper, the overall simulation model of the system is built in MATLAB/Simulink, as shown in Figure 8.

The given torque $T^* = 600$ Nm, the load torque $T_\mathrm{L} = 20$ Nm, and the acceleration is started from the rotational speed of 0 until the maximum speed limit of 3500 rpm. The velocity waveform is shown in Figure 9. The torque given waveform is shown in Figure 10. The output torque waveform is shown in Figure 11, wherein the three-phase current waveform of the first group of stator windings is as shown in Figure 12. Figure 9 shows that the speed limiter ring can effectively limit the speed. Figure 10 shows that the BP neural network-based optimal efficiency torque distribution method

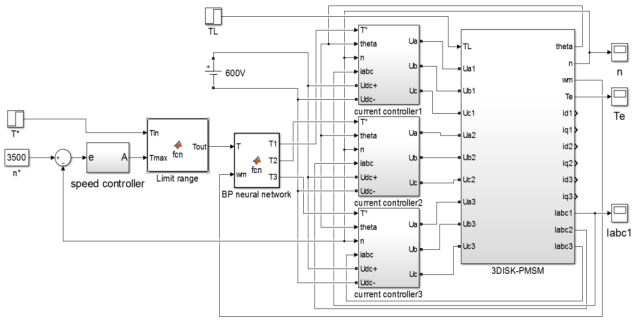

FIGURE 8. System overall simulation model.

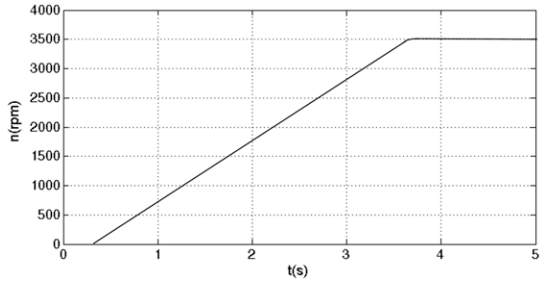

FIGURE 9. System overall simulation model.

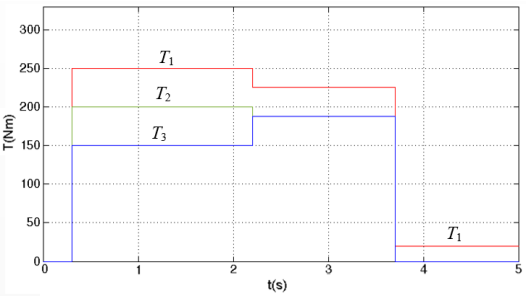

FIGURE 10. Speed response waveform.

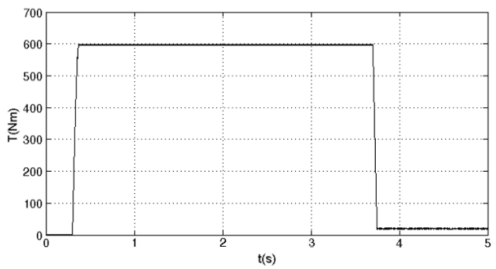

FIGURE 11. Torque reference waveform.

proposed in this paper can reasonably distribute the torque. Figures 11 and 12 show that the vector control based on the deadbeat current prediction controller has fast response capability and good reliability and stability.

B. DRIVE SYSTEM EXPERIMENT

The drive system experiment was completed on a 160 kW motor-to-drag test platform, and the drag-and-drop test platform is shown in Figure 13.

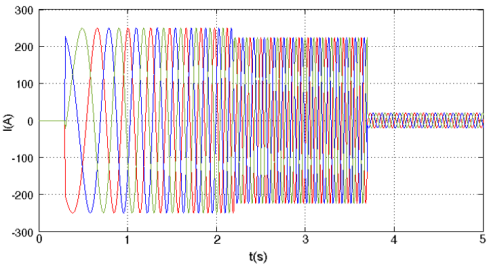

FIGURE 12. Output torque waveform.

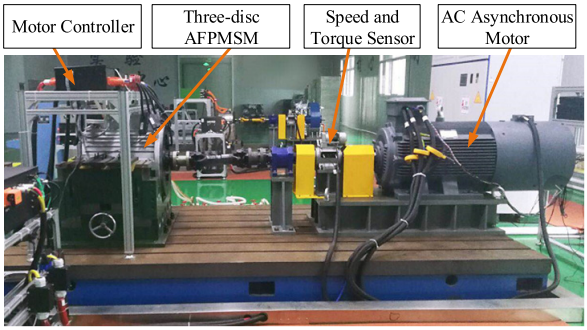

FIGURE 13. Drag and drop experimental platform.

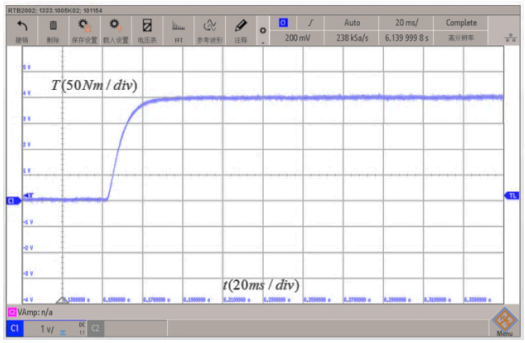

FIGURE 14. System torque tracking waveform based on PI controller.

First, a torque tracking experiment was performed to verify the proposed current controller performance based on the deadbeat current prediction control. The three-disc AFPMSM operates in a single-disc mode with only one set of motor controllers. The host computer software sends a torque command to the motor controller through the controller area network (CAN) bus. The torque sensor feeds back the torque information, outputs the analog quantity, and the oscilloscope is used to read, save and analyze the torque information. The sensor ratio is 50Nm/1V. The torque follow-up experiments were carried out on the drive control system based on the PI controller and the design based on the deadbeat current predictive controller. The abrupt torque is given as 200Nm, and the feedback torque waveform is shown in Figure 14 and Figure 15.

It can be seen from Figure 14 and Figure 15 that, based on the proportional integral (PI) controller's drive system, the time taken for the torque to reach a steady state from

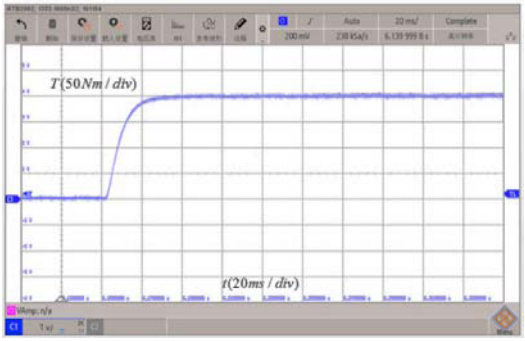

FIGURE 15. System torque tracking waveform based on deadbeat current prediction controller.

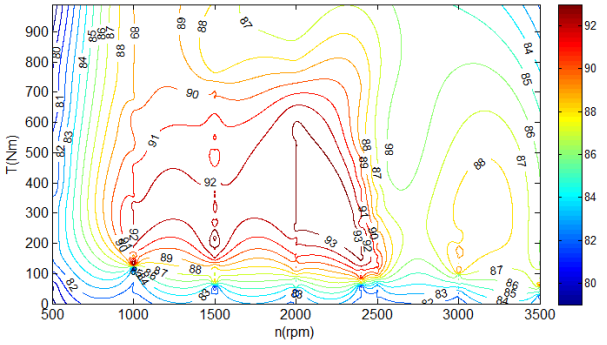

FIGURE 16. System MAP in torque three-division mode.

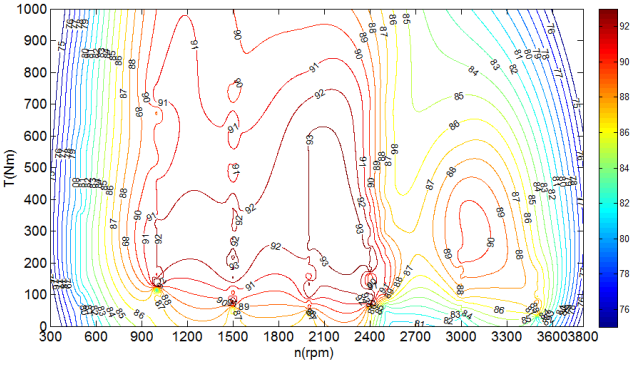

FIGURE 17. System efficiency MAP based on BP neural network for optimal efficiency distribution method.

FIGURE 18. Experimental electric bus.

0 Nm to 200 Nm is about 42ms, and there is a certain overshoot. Based on the deadbeat current prediction controller's drive system, the time taken for the torque to reach a steady state from 0Nm to 200Nm is about 34ms, and there is no torque overshoot, and the torque ripple is small at steady state. The experimental results show that the designed current controller based on the deadbeat current prediction control can improve the dynamic performance of the system torque tracking and reduce the torque ripple during steady-state operation, which meets the expected requirements.

Then drive the system efficiency experiment. On the motor-to-drag experiment platform, the BP neural network-based torque distribution method was used to test the efficiency. The output torque T and the rotational speed n on the three-disc AFPMSM rotor shaft are acquired by the torque and speed sensors, and then the input voltage U and the current I of the DC side of the motor controller are collected by a storage recording instrument. System efficiency η is:

$$\eta = \frac{2\Omega}{60} \cdot \frac{Tn}{UI} \tag{34}$$

The maximum speed of the motor is 3500 rpm. In order to test the motor performance, from the motor speed of 300 rpm to 3800 rpm, a speed point is selected every 100 rpm for a total of 36 speed points. At each speed point, from the output torque 0Nm to 990Nm, a torque point is selected every 50Nm for a total of 20 torque points. Corresponding to different speeds and torques, a total of 720 efficiency collection points are set, and the output torque T, the rotation speed n, the DC side input voltage U and the current I of each efficiency point are collected, and then the driving system efficiency is calculated by Equation 38. Then, the output torque T, the rotational speed n and the system efficiency n are imported into MATLAB, and the motor system efficiency MAP can be generated. The system efficiency MAP is shown in Figure 16-17.

It can be seen from Figure 16 that the efficiency of the motor is only high in the vicinity of the rated speed, and the efficiency is relatively low in other areas. It can be seen from Figure 17 that when the motor speed is 900 to 2500 rpm and the torque is 100 to 900 Nm, the system efficiency is above 90%. In addition, when the motor speed is 3000 to 3200 rpm and the torque is 200 to 400 Nm, the system efficiency is also close to 90%. The experimental results show that the BP neural network based torque distribution method can effectively improve the efficiency of the drive system.

C. VEHICLE EXPERIMENT

The electric bus used for the three-disc AFPMSM loading experiment is shown in Figure 18. The electric bus is 12m long, 2.5m wide and 3m high. The three-disc AFPMSM is shown in Figure 19(a), one of the motor controller is shown in Figure 19(c), and the power battery pack is shown in Figure 19(b).

The electric bus has an unloaded weight of about 15 tons, a power battery pack capacity of 400 Ah, a charging capacity

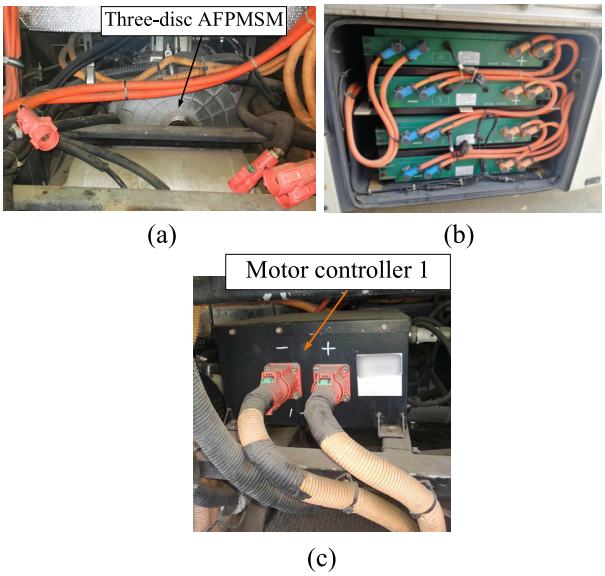

FIGURE 19. Electric bus internal structure. (a) The three-disc AFPMSM, (b) the power battery pack, (c) the motor controller.

TABLE 1. Electric bus cruising range.

Experimental Condition	Distribution-Based Torque Distribution Method	Efficiency Optimal Torque Distribution Method Based on BP Neural Network
No Load	245km	281km
2 Tons Load	211km	243km

of 225 kWh, and a design speed of 60 km/h. Experiments were carried out with the experimental electric bus shown in Figure 18, and the endurance capability under the base-allocated torque distribution method and the BP neural network-based torque distribution method were tested. In the urban roads, the battery life of the electric bus under no-load and 2 tons load (about 30 people) was tested separately. The experimental data is shown in Table 1.

It can be seen from Table 1 that the three-disc AFPMSM drive system for electric buses designed in this paper has a higher cruising range in the actual operation of electric buses. The BP neural network-based torque distribution method can increase the cruising range by about 15% under no-load and 2 ton load conditions compared to the average distribution-based torque distribution method. Experiments show that the BP neural network based torque distribution method can effectively improve system efficiency, save energy and increase cruising range.

VI. CONCLUSION

In this paper, the three-stator-double rotor AFPMSM is taken as the research object, and the deadbeat current predictive vector control system based on the efficiency optimal torque distribution method is studied. The following conclusions can be drawn:

1.The results of the overall drive simulation show that the drive control system designed in this paper can meet the needs of practical applications.

2. The motor-to-drag experiment platform and the whole vehicle experiment show that the BP neural network-based torque distribution method can effectively improve the system high efficiency range. Compared with the method of torque average distribution, the BP neural network based distribution method can increase the cruising range by about 15% under both no-load and 2 ton load conditions.

3. The drive system based on the deadbeat current prediction controller can effectively improve the torque tracking characteristics. The motor-to-drag experiment shows that when the torque changes from 0Nm to 200Nm, the time taken for the drive system based on the deadbeat-free current prediction controller to reach a steady state is less than the conventional PI control, and there is no torque overshoot, and torque ripple is small at steady state.

In addition to the above research content, there are still some content worthy of further research and optimization. If the influence of the flux linkage between the three sets of stator windings and between the two sets of permanent magnet rotors is considered, the system performance will be further improved. In addition, in order to further improve the cruising range of electric buses, the related control strategies for energy recovery can be studied in the future.

REFERENCES

[1] D. Liyuan, Q. Yue, W. Wenjing, and Q. Guoliang, "Current situation of energy saving and emission reduction of urban public transportation and green development suggestion," in *Proc. IEEE ICITBS*, Changsha, China, Dec. 2016, pp. 14–17.
[2] M. Zhu, X.-Y. Liu, F. Tang, M. Qiu, R. Shen, W. Shu, and M.-Y. Wu, "Public vehicles for future urban transportation," *IEEE Trans. Intell. Transp. Syst.*, vol. 17, no. 12, pp. 3344–3353, Dec. 2016.
[3] X. Sun, C. Hu, J. Zhu, S. Wang, W. Zhou, Z. Yang, G. Lei, K. Li, B. Zhu, and Y. Guo, "MPTC for PMSMs of EVs with multi-motor driven system considering optimal energy allocation," *IEEE Trans. Magn.*, vol. 55, no. 7, Jul. 2019, Art. no. 8104306.
[4] Z. Shi, X. Sun, Y. Cai, Z. Yang, G. Lei, Y. Guo, and J. Zhu, "Torque analysis and dynamic performance improvement of a PMSM for EVs by skew angle optimization," *IEEE Trans. Appl. Supercond.*, vol. 29, no. 2, pp. 1–5, Mar. 2019.
[5] X. Tang, W. Yang, X. Hu, and D. Zhang, "A novel simplified model for torsional vibration analysis of a series-parallel hybrid electric vehicle," *Mech. Syst. Signal Process.*, vol. 85, pp. 329–338, Feb. 2017.
[6] X.-L. Tang, X. Hu, W. Yang, and H. Yu, "Novel torsional vibration modeling and assessment of a power-split hybrid electric vehicle equipped with a dual-mass flywheel," *IEEE Trans. Veh. Technol.*, vol. 67, no. 3, pp. 1990–2000, Mar. 2018.
[7] M. Aydin, M. Gulec, Y. Demir, B. Akyuz, and E. Yolacan, "Design and validation of a 24-pole coreless axial flux permanent magnet motor for a solar powered vehicle," in *Proc. IEEE 22nd ICEM*, Lausanne, Switzerland, Sep. 2016, pp. 1493–1498.
[8] J. Zhao, B. Li, and Z. Gu, "Research on an axial flux PMSM with radially sliding permanent magnets," *Energies*, vol. 8, no. 3, pp. 1663–1684, Mar. 2015.
[9] A. Hemeida, P. Sergeant, A. Rasekh, H. Vansompel, and J. Vierendeels, "An optimal design of a 5MW AFPMSM for wind turbine applications using analytical model," in *Proc. IEEE 22nd ICEM*, Lausanne, Switzerland, Sep. 2016, pp. 1290–1297.
[10] Y. Pei, Q. Wang, Y. Bi, and F. Chai, "A novel structure of axial flux permanent magnet synchronous machine with high torque density for electrical vehicle applications," in *Proc. IEEE 43rd IECON*, Beijing, China, Oct. 2017, pp. 1717–1722.

[11] D.-K. Lim, Y.-S. Cho, J.-S. Ro, S.-Y. Jung, and H.-K. Jung, "Optimal design of an axial flux permanent magnet synchronous motor for the electric bicycle," *IEEE Trans. Magn.*, vol. 52, no. 3, Mar. 2016, Art. no. 8201204.
[12] Q. Chen, D. Liang, L. Gao, Q. Wang, and Y. Liu, "Hierarchical thermal network analysis of axial-flux permanent-magnet synchronous machine for electric motorcycle," *IET Electr. Power App.*, vol. 12, no. 6, pp. 859–866, Jul. 2018.
[13] Y. Zhang, N. Liu, S. Guo, J. Tong, and Q. Zhou, "Analysis and design of ironless axial flux permanent magnet synchronous motor," in *Proc. IEEE 10th IHMSC*, Hangzhou, China, Aug. 2018, pp. 170–173.
[14] S. Neethu, K. S. Shinoy, and A. S. Shajilal, "Efficiency improvement of an axial flux permanent magnet brushless DC motor for LVAD application," *Appl. Mech. Mater.*, vols. 110–116, pp. 4661–4668, Oct. 2012.
[15] S. A. Fayazi and A. Vahidi, "Mixed-integer linear programming for optimal scheduling of autonomous vehicle intersection crossing," *IEEE Trans. Intell. Veh.*, vol. 3, no. 3, pp. 287–299, Sep. 2018.
[16] C. Yang, W. Lou, J. Yao, and S. Xie, "On charging scheduling optimization for a wirelessly charged electric bus system," *IEEE Trans. Intell. Transp. Syst.*, vol. 19, no. 6, pp. 1814–1826, Jun. 2018.
[17] K. Kivekäs, J. Vepsäläinen, and K. Tammi, "Stochastic driving cycle synthesis for analyzing the energy consumption of a battery electric bus," *IEEE Access*, vol. 6, pp. 55586–55598, 2018.
[18] L. Li, C. Yang, Y. Zhang, L. Zhang, and J. Song, "Correctional DP-based energy management strategy of plug-in hybrid electric bus for city-bus route," *IEEE Trans. Veh. Technol.*, vol. 64, no. 7, pp. 2792–2803, Jul. 2015.
[19] X. Tian, R. He, and Y. Xu, "Design of an energy management strategy for a parallel hybrid electric bus based on an IDP-ANFIS scheme," *IEEE Access*, vol. 6, pp. 23806–23819, 2018.
[20] W. Wang, J. Shi, Z. Zhang, and C. Lin, "Optimization of a dual-motor coupled powertrain energy management strategy for a battery electric bus," *Energy Procedia*, vol. 145, pp. 20–25, Jul. 2018.
[21] C. Gan, N. Jin, Q. Sun, W. Kong, Y. Hu, and L. M. Tolbert, "Multiport bidirectional SRM drives for solar-assisted hybrid electric bus powertrain with flexible driving and self-charging functions," *IEEE Trans. Power Electron.*, vol. 33, no. 10, pp. 8231–8245, Oct. 2018.
[22] J. Li, M. Zhang, Q. Yang, Z. Zhang, and W. Yuan, "SMES/battery hybrid energy storage system for electric buses," *IEEE Trans. Appl. Supercond.*, vol. 26, no. 4, pp. 1–5, Jun. 2016.
[23] D. Zhang, S. Zhang, T. Fan, and X. Wen, "Modeling and estimation for conducted common-mode interference of a motor drive system used in electric vehicle," in *Proc. IEEE 21st ICEMS*, Jeju, South Korea, Oct. 2018, pp. 831–835.
[24] C. Li, W. Huang, R. Cao, F. Bu, and C. Fan, "An integrated topology of charger and drive for electric buses," *IEEE Trans. Veh. Technol.*, vol. 65, no. 6, pp. 4471–4479, Jun. 2016.
[25] J. Zhao, M. Hua, and T. Liu, "Research on a sliding mode vector control system based on collaborative optimization of an axial flux permanent magnet synchronous motor for an electric vehicle," *Energies*, vol. 11, no. 11, p. 3116, Nov. 2018.
[26] X. Sun, C. Hu, G. Lei, Y. Guo, and J. Zhu, "State feedback control for a pm hub motor based on grey wolf optimization algorithm," *IEEE Trans. Power Electron.*, to be published. doi: 10.1109/TPEL.2019.2923726.
[27] J. Huang, Y. Liu, M. Liu, M. Cao, and Q. Yan, "Multi-objective optimization control of distributed electric drive vehicles based on optimal torque distribution," *IEEE Access*, vol. 7, pp. 16377–16394, 2019.
[28] L. Chen, T. Chen, X. Xu, Y. Cai, H. Jiang, and X. Sun, "Multi-objective coordination control strategy of distributed drive electric vehicle by orientated tire force distribution method," *IEEE Access*, vol. 6, pp. 69559–69574, Oct. 2018.
[29] P. C. Krause, O. Wasynczuk, and S. D. Sudhoff, *Analysis of Electric Machinery and Drive Systems*. New York, NY, USA: IEEE Press, 2013. [Online]. Available: https://ieeexplore.ieee.org/book/6712180

JIANFEI ZHAO received the B.S. and M.S. degrees in mechatronic engineering from Xi'an Jiaotong University, Xi'an, China, in 2000 and 2003, respectively, and the Ph.D. degree in electrical engineering from Shanghai Jiao Tong University, Shanghai, China, in 2012.

From 2003 to 2006, he was a Research and Development Engineer and a Project Manager with the Research and Development Center of Myway-labs Company Ltd., Japan. Since 2012, he has been an Assistant Professor with the Mechatronic Engineering and Automation School, Shanghai University. His research interests include power electronics and electric vehicles.

LIXIAO ZHENG received the B.S. degree in electrical engineering and automation from Shanghai University, Shanghai, China, in 2019, where she is currently pursuing the M.S. degree in electrical engineering. Her research interests include electric vehicle drive control and new energy generation.

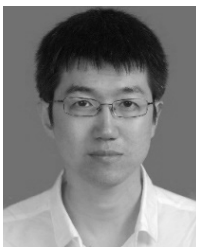

SHUANG WANG was born in Jilin, China, in 1977. He received the B.S., M.S., and Ph.D. degrees in electrical engineering from the Harbin Institute of Technology, Harbin, China, in 2000, 2005, and 2009, respectively. Since 2010, he has been with the School of Mechatronic Engineering and Automation, Shanghai University, Shanghai, China, where he is currently an Assistant Professor. His current research interests include intelligent control theory and its application to new energy vehicles, power electronics, and servo control systems.

MINQI HUA received the B.S. degree from Shanghai University, Shanghai, China, in 2018, where she is currently pursuing the M.S. degree with the Mechatronic Engineering and Automation School. Her research interests include electric vehicle drive control and new energy generation.